Engineering Fracture Mechanics 178 (2017) 77–92

Contents lists available at ScienceDirect

Engineering Fracture Mechanics

journal homepage: www.elsevier.com/locate/engfracmech

Revised wide range compliance solutions for selected standard and non-standard fracture test specimens based on crack mouth opening displacement

Rodolfo F. de Souza, Claudio Ruggieri *

Department of Naval Architecture and Ocean Engineering, University of São Paulo, São Paulo, Brazil

ARTICLE INFO

Article history:
Received 30 October 2016
Received in revised form 11 April 2017
Accepted 11 April 2017
Available online 17 April 2017

Keywords:
Compliance solutions
Crack length evaluation
Unloading compliance
CMOD
Fracture specimens

ABSTRACT

This work addresses the development of wide range compliance solutions for tensile-loaded and bend specimens based on CMOD. The study covers selected standard and non-standard fracture test specimens, including the compact tension C(T) configuration, the single edge notch tension SE(T) specimen with fixed-grip loading (clamped ends) and the single edge notch bend SE(B) geometry with varying specimen span over width ratio and loaded under 3-point and 4-point flexural configuration. Very detailed elastic finite element analysis in 2-D setting are conducted on fracture models with varying crack sizes to generate the evolution of load with displacement for those configurations from which the dependence of specimen compliance on crack length, specimen geometry and loading mode is determined. To examine 3-D effects, including the influence of side-grooves, on the specimen compliance response, numerical analyses are also performed on 3-D models of selected plane-sided and side-grooved fracture specimens. The extensive numerical analyses conducted here provide a large set of compliance solutions, which not only validate the compliance relationships available in existing standards, but also help consolidating elastic compliance functions of common specimen geometries for use in routine test procedures for experimental evaluations of crack size changes in fracture toughness and fatigue crack growth testing.

1. Introduction

Fracture mechanics based approaches to describe ductile fracture behavior of structural components in the upper-shelf region generally rely upon crack growth resistance curves ($J-\Delta a$ or, equivalently, CTOD $-\Delta a$) to characterize crack extension followed by crack instability of the material. Here, the fracture resistance curve (also termed R-curve) is defined in terms of the J-integral or the crack-tip opening displacement (CTOD) representing the crack driving force and Δa as the amount of crack growth [1,2]. Under sustained ductile tearing of a macroscopic crack, large increases in the load-carrying capacity for the flawed structural component are possible beyond the limits given by the load levels at yielding of the remaining crack ligament. Retaining contact with traditional approaches, advanced procedures for defect assessments, particularly Engineering Critical Assessment (ECA) methodologies, make extensive use of the significant increases in toughness of ductile steels and aluminum alloys during ductile crack growth to specify acceptable flaw sizes for safe operation and life extension

* Corresponding author.
E-mail address: claudio.ruggieri@usp.br (C. Ruggieri).

http://dx.doi.org/10.1016/j.engfracmech.2017.04.013
0013-7944/

Nomenclature

α_k	coefficients for the polynomial fitting defining the relationship between μ and a/W
β_k	coefficients for the polynomial fitting defining the relationship between a/W and μ
Δ	load line displacement
Δa	amount of stable crack growth
η	plastic η-factor to determine the plastic component of J
μ	normalized specimen compliance
ν	Poisson's ratio
ρ_0	radius of the initial blunt notch at the crack tip
a	crack depth
A_p	plastic component of the area under the load-CMOD curve
B	specimen thickness
B_e	effective specimen thickness
B_N	net specimen thickness
C	specimen compliance
C_V	CMOD-based compliance
C_Δ	LLD-based compliance
D	inner specimen span
E	Young's modulus
G	strain energy release rate
H	distance between clamped grips for the clamped SE(T) specimen
J	J-integral
J_p	plastic component of the J-integral
J_c	J-value at cleavage instability
K	elastic stress intensity factor
K_{Ic}	critical value of Mode I elastic stress intensity factor
P	applied (remote) load
R	crack growth resistance curve
S	specimen span
V	crack mouth opening displacement
W	specimen width
X, Y, Z	Cartesian coordinates
ASTM	American Society for Testing and Materials
C(T)	compact tension
CMOD	crack mouth opening displacement
CTOD	crack tip opening displacement
ECA	engineering critical assessment
ISO	International Organization for Standardization
LLD	load line displacement
SCR	steel catenary riser
SE(B)	single edge notch bend
SE(T)	single edge notch tension
UC	unloading compliance
1T	standard specimen thickness corresponding to 1 in. (25.4 mm)

programs of in-service structures. Deep water steel catenary risers (SCRs) installed by the pipe reeling process, in which the welded pipe is coiled around a large diameter reel on a vessel and then unreeled, straightened and finally deployed to the sea floor [3–6], provide an example in that flaw acceptance criteria for pipeline girth welds allow significant amounts of stable crack growth with increased loading to determine tolerable flaw sizes [7].

Conventional testing programs to measure crack growth resistance curves in ductile materials employ primarily the unloading compliance (UC) procedure using a single specimen test in which evaluation of the instantaneous value of specimen compliance at partial unloading during the fracture test simply derives from directly measuring the applied load and specimen deformation, which can be defined either in terms of the load-line displacement (LLD) or crack mouth opening displacement (CMOD). Because of its relative ease with which the load-displacement records can be measured in conventional test specimens, the method represents a key step in testing protocols measuring fracture resistance response in ductile materials such as ASTM E1820 [8]. Another application of interest for the compliance method remains in experimental

measurements of crack length and crack closure during fatigue crack growth testing [9–13]. However, application and extensions of the UC procedure to accurately estimate crack length from experimental load-displacement records rely strongly on known functional forms describing the relationship between crack size and specimen compliance for crack configurations spanning a wide range of geometries and crack sizes.

Early progress in developing elastic compliance functions for common fracture specimens was achieved in the work of Saxena and Hudak [14]. They focused on formulating compliance expressions for compact tension C(T) geometries in terms of LLD measurements by integrating stress intensity factor solutions with respect to the crack length. Subsequently, Wu [15], Haggag and Underwood [16] and Underwood et al. [17] developed elastic compliance solutions for three-point bend specimens on the basis of known relationships between load and load-line displacements for cracked bend bars [18]. Other research efforts have focused on developing more extensive compliance solutions applicable to several other crack geometries, including non-standard fracture specimens, most of them by making recourse to numerical analyses based on the finite element method to determine a linear relationship between applied load and displacement (either characterized in terms of LLD or CMOD). These studies include the earlier works of Papaspyropoulos and Ahmad [19], Blatt et al. [20], Tobler and Carpenter [21], Jablonski et al. [22], Kapp et al. [23], Tarafder et al. [24], John [25] and Guinea et al. [26], as well the more recent studies of Joyce et al. [27], Cravero and Ruggieri [28], Shen and Tyson [29], Mathias et al. [30], among others. In related work, Verstraete et al. [31] performed elastic-plastic finite element analyses on 3-D numerical models for clamped SE(T) specimens having side-grooves to determine the potential effects of plastic deformation on the actual specimen compliance. Their study provides insights into the role of plastic deformation, particularly that associated with crack-tip blunting, on the early part of a fracture resistance curve for an X80 pipeline steel, including the apparent negative crack growth often observed in fracture resistance testing of ductile materials (see, *e.g.*, Sarzosa et al. [32] for an illustrative example of apparent negative crack growth that arises in fracture resistance testing of a pipeline girth weld). However, in the present work we pursue a line of investigation in which wide range elastic compliance solutions of common fracture specimens are revised and extended for use in fracture test procedures.

In retrospect, much of the earlier development of compliance solutions for common fracture specimens was made in terms of a linear relationship between applied load and load-line displacement (LLD). This is consistent with the methodology to evaluate J with crack extension which derives from a stability analysis of J-controlled crack growth using the measured load-load line displacement records. Indeed, by using the energy release rate definition of J for a cracked body [2,33] and, further, upon interpretation of the plastic area under the load versus load-line displacement, represented here by A_p^{LLD}, as the plastic contribution to the strain energy (due to the crack), there is a rigorous relationship between J and A_p [33–36]. This conclusion embodies a large part of the earlier progress in fracture resistance testing protocols and provided the basis for current fracture test standards incorporating J-resistance evaluation procedures (see Joyce [37] and the review paper of Zhu and Joyce [38]). However, much current research favors the direct use of experimental measurements of load and crack mouth opening displacements (CMOD) to generate crack growth resistance curves. While there are essentially no significant differences between J or Δa derived from experimental measurements based on either load-load line displacements or load-crack mouth opening displacements, even in the case of bend specimens (see, *e.g.*, Faucher and Tyson [39]), it is also recognized that J and Δa can be evaluated more easily with a clip gage mounted at the crack mouth of most fracture specimens, including the bend specimen and the single edge notch tension geometry. Moreover, while all those previously mentioned works share commonly the essential features of a linear relationship between applied load and displacement (either LLD or CMOD), their compliance solutions were derived on the basis of somewhat different numerical techniques, including direct integration of stress intensity expressions. Perhaps more importantly, there are no systematic studies addressing the development of compliance solutions for standard and non-standard fracture specimens using a common numerical framework which can, therefore, provide a uniform body of results against which other published results can be compared (and possibly enlarged). Given the current standardization scenario in which non-standard fracture specimens are increasingly being utilized in routine fracture toughness testing, development of a more extensive and comprehensive set of compliance solutions appears largely justified.

This work addresses the development of wide range compliance solutions for tensile-loaded and bend specimens based on CMOD. The study covers selected standard and non-standard fracture test specimens, including the compact tension C(T) configuration, the single edge notch tension SE(T) specimen with fixed-grip loading (clamped ends) and the single edge notch bend SE(B) geometry with varying specimen span over width ratio and loaded under 3-point and 4-point flexural configuration. Detailed elastic finite element analysis in 2-D setting are conducted on fracture models with varying crack sizes to generate the evolution of load with displacement for those configurations from which the dependence of specimen compliance on crack length, specimen geometry and loading mode is determined. To examine 3-D effects, including the influence of side-grooves, on the specimen compliance response, numerical analyses are also performed on 3-D models of selected plane-sided and side-grooved fracture specimens. The extensive numerical analyses conducted here provide a large set of compliance solutions, which not only validate the compliance relationships available in existing standards, but also help consolidating elastic compliance functions of common specimen geometries for use in routine test procedures for experimental evaluations of crack size changes in fracture toughness and fatigue crack growth testing.

2. Elastic compliance and geometry of fracture test specimens

The relationship between displacement, as generally characterized by the load line displacement (LLD or Δ) or, equivalently, the crack mouth opening displacement (CMOD or V), and applied load corresponding to linear elastic behavior defines the elastic compliance for a cracked body, denoted as C, illustrated in Fig. 1, including standard and non-standard fracture specimens. With increased crack size, a, the ratio $C_\Delta = \Delta/P$ (or, equivalently, $C_V = V/P$) increases, as depicted in Fig. 1(b), which simply reflects a decreasing stiffness of the cracked body (since this quantity is the inverse of the compliance). These changes in the relationship between load and crack displacement provide a simple and yet highly effective, indirect method to accurately estimate crack length and to measure the amount of crack growth in routine fracture testing using a variety of fracture specimen geometries, such as J-resistance curve testing [8,28,30] and fatigue crack growth testing [9]. Here, development of accurate and wide-range expressions relating C and crack size represents a key step in compliance-based crack length measurement techniques.

Early progress in developing analytical compliance functions for non side-grooved specimen geometries was driven by the relationship between the LLD-based compliance, C_Δ, and energy release rate, G, in the form $G = f(dC_\Delta/da)$, in which a is the crack size [2,40]. By manipulating this dependence of G on C_Δ and making use of the standard relationship given by $G = K^2/E'$, in which K defines the elastic stress intensity factor and $E' = E$ or $E' = E/(1-\nu^2)$ whether plane-stress or plane-strain conditions apply with E denoting the Young's modulus and ν is the Poisson's ratio, the change in specimen compliance with crack size is expressed as [40]

$$\frac{KB\sqrt{W}}{P} = F(a/W) = \left[\frac{1}{2}\frac{d(C_\Delta BE')}{d(a/W)}\right]^{1/2} \tag{1}$$

which provides a relatively simple procedure to determine experimental values of K by measuring the compliance change with crack size for any specimen geometry or it can be solved for the specimen compliance, C_Δ, once the stress intensity factor solution for the specimen geometry is known. In the above, B is the specimen thickness and W represents the specimen width. Later, Saxena and Hudak [14] have generalized the elastic compliance relations in the form

$$a/W = f(\mu) \tag{2}$$

where μ defines a normalized compliance in terms of C, specimen dimension B and the material property E' so that it becomes independent of specimen size and material. Adoption of a normalized form for the specimen compliance facilitates the development of more convenient polynomial functions describing the above Eq. (2) as given later. It is also of interest to note that the above elastic compliance relation can be determined with μ defined in terms of plane-strain conditions and then used to evaluate the crack length under plane-stress conditions by simply resetting the elastic modulus from $E' = E/(1-\nu^2)$ to $E' = E$. Further discussion of this issue is deferred to Section 4.6 later in this article.

This section provides details for the geometry of the fracture test specimens analyzed in this work to derive elastic compliance solutions as a function of a/W as well as their inverse. The formulation and terminology adopted here follows closely whenever possible ASTM E1823 [41] and ASTM E1820 [8]. The description begins with predominantly tensile-loaded specimens, including the compact tension C(T) specimen and the single edge notch tension SE(T) specimen. Subsequent presentation focuses on the standard and non-standard single notch bend SE(B) specimen under 3-point and 4-point loading. The

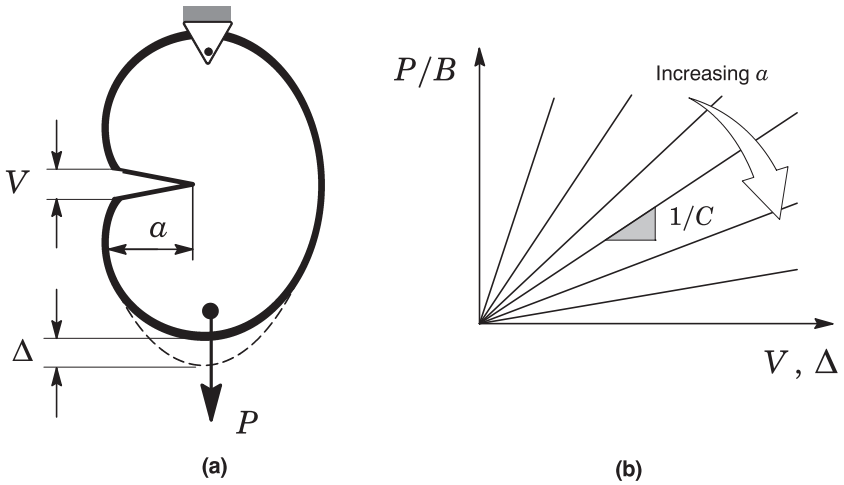

Fig. 1. (a) Arbitrary cracked body with thickness B subjected to remote loading, P, in which V defines the crack mouth opening displacement (CMOD) and Δ represents the load-line displacement (LLD); (b) Linear relationship between applied load normalized by thickness and displacement with varying crack size.

presentation that follows is centered on the crack mouth opening displacement (CMOD) as the primary measured quantity describing the displacement of the crack configuration. For simplicity, we hereafter refer to C as the specimen compliance in terms of CMOD.

2.1. Tensile-loaded specimens

The compact tension C(T) specimen is perhaps the most extensively used crack configuration in fracture testing, including fracture toughness and fatigue crack growth measurements [9,8]. Earlier versions of ASTM E1820 [8] recommended the use of two slightly different geometries according to the type of required fracture test. For K_{Ic} testing, the specimen is equipped with a straight machined notch as illustrated in Fig. 2(a) since only CMOD is measured during the test. ASTM E647 [9] also adopts an essentially similar geometry in fatigue crack growth rate testing. Here, a is the crack size and W represents the specimen width. Recent versions of ASTM E1820 [8] dropped the compact tension specimen with a straight notch and adopted the C(T) geometry with a cutout in the original notch to facilitate knife-edge positioning at the load line (thereby allowing a relatively simple measurement of the load-line displacement) as the preferred configuration for J-integral testing.

Adoption of the latter configuration, however, derives from the early development of J-integral testing [34,42,33] in which J is directly connected to the plastic contribution to the strain energy (due to the crack) expressed in terms of load line displacement (LLD) measurements by means of a non-dimensional plastic η-factor [43,33]. While there is a rigorous relationship between the area under the load versus load-line displacement (which represents the plastic contribution to the strain energy for the cracked body with J), Cravero and Ruggieri [36] and Zhu et al. [44] have shown that there also exists a direct connection between the plastic component of J and the plastic work of applied load in terms of CMOD. Thus, recent progress to support the development of fracture toughness test procedures, including experimental measurements of the J-integral at cleavage instability, J_c, and J-resistant curves, favor the use of CMOD (rather than LLD) due to simpler specimen machining and easier knife-edge positioning associated with the configuration displayed in Fig. 2(a) – this geometry is used in the present study to derive CMOD-based compliance solutions as addressed later. Further, Kirk and Dodds [45] have also shown that the η-factors needed to determine J are much less sensitive to the hardening properties when the plastic area is computed from CMOD rather than LLD.

Another tensile-loaded crack configuration which is gaining increased interest in fracture mechanics applications is the single edge notch tension SE(T) specimen with fixed-grip loading [46–49]. This specimen configuration has been increasingly used in crack growth resistance measurements for key structural applications in low constraint conditions, including girth weld defect assessments in oil and gas transmission pipelines and submarine risers [50,51]. Fig. 2(b) displays the geometry of

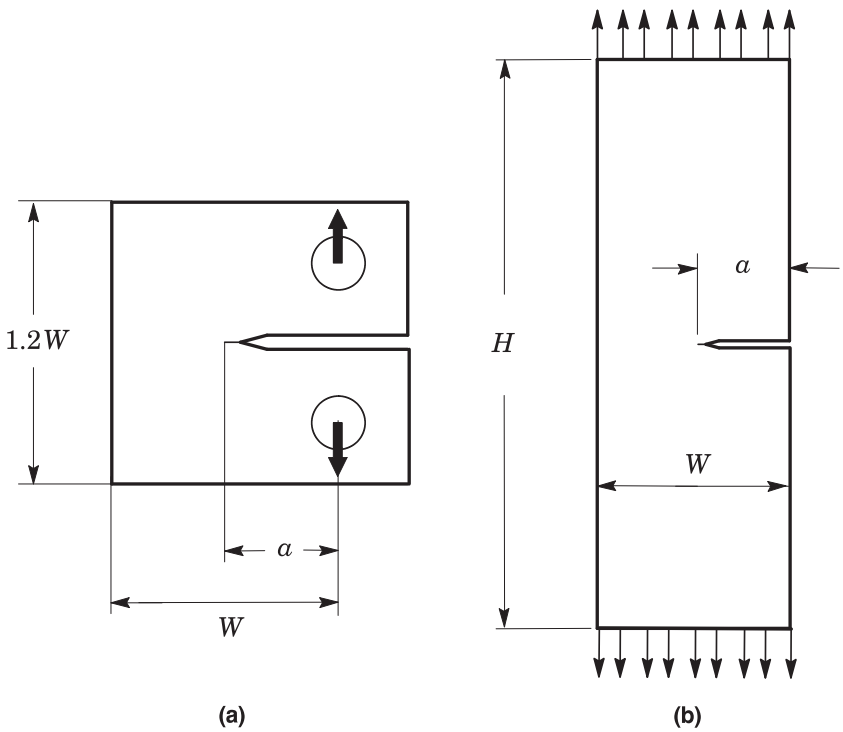

Fig. 2. Tensile-loaded geometries: (a) Compact tension C(T) specimen with straight machined notch. (b) Single edge notch tension SE(T) specimen with fixed-grip loading (clamped ends).

conventional SE(T) fracture specimens under clamped end conditions in which H defines the distance between the clamped grips.

For the crack configurations discussed above, the normalized specimen compliance based on CMOD is most often expressed as

$$\mu_{CT} = \mu_{SET} = \left[1 + \sqrt{E' B_e C}\right]^{-1} \tag{3}$$

in which the effective thickness, B_e, is defined by

$$B_e = B - \frac{(B - B_N)^2}{B} \tag{4}$$

where B_N is the net specimen thickness at the side groove roots ($B_N = B$ if the specimen has no side grooves where B is the specimen gross thickness).

2.2. Single edge notch bend specimens

Single edge notch bend SE(B) specimens are also extensively used in fracture toughness testing of various structural materials. The prevailing geometry is the 3-point bend configuration shown in Fig. 3(a) in which S is the specimen span (distance between the roller supports). Most fracture test standards, including ASTM E1820 [8], BS 7448 [52] and ISO 12135 [53], adopt a conventional 3-point SE(B) geometry with $S = 4W$.

Another convenient bend test configuration, albeit not yet standardized, which has gained practical importance in fatigue testing of various metallic alloys [54–57] is the 4-point bend geometry displayed in Fig. 3(b) in which D represents the inner span. Here, the flexural bend test fixture produces a uniform moment between the two inner loading rollers in the specimen (and associated zero shear stress) as can be easily verified by using simple beam flexure theory [58,59].

For the bend specimens under consideration, the normalized specimen compliance based on CMOD can be expressed as

$$\mu_{SEB} = \left[1 + \sqrt{4E' B_e C W / S}\right]^{-1} \tag{5}$$

in which B_e was already defined. The above expression reduces to previous Eq. (3) in case of the standard 3-point bend geometry with $S = 4W$.

3. Computational procedures

3.1. 2-D finite element models

Extensive finite element analyses are performed on plane-strain models for the tensile-loaded and bending loading configurations described previously covering a wide range of specimen geometries and varying crack sizes. The analysis matrix builds upon a 1T reference thickness ($B = 25.4$ mm) to define a conventional specimen width of $W = 2B = 50.8$ mm for all models (refer to Section 2 and associated figures displaying the geometry and specimen dimensions for the analyzed crack configurations) and includes: (1) a C(T) specimen with straight notch; (2) a clamped SE(T) configuration with $H/W = 10$; (3) 3-point SE(B) geometries with $S/W = 4$, 6 and 8 and (4) 4-point SE(B) specimens with $S/W = 4$, 6 and 8 having a inner span

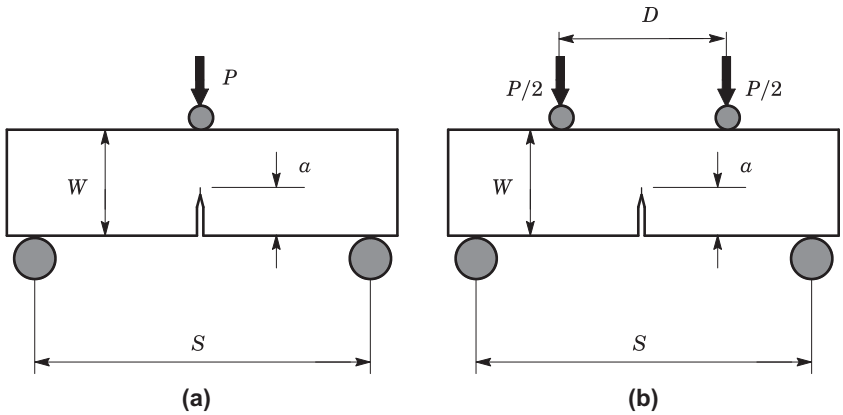

Fig. 3. Conventional bending loading geometries: (a) 3-point SE(B) specimen. (b) 4-point bend specimen.

$D = S/2$. The finite element models for all analyzed specimen geometries cover a range of a/W from 0.1 ~ 0.8 with increments of 0.1.

Fig. 4(a) and (b) shows the finite element models constructed for the plane-strain analyses of the 3P SE(B) specimen and clamped SE(T) geometry having $a/W = 0.5$. All other crack models have very similar features and are not shown here in interest of space. Because of the elastic character of the finite element computations reported in the present study, special attention in terms of crack tip mesh details or very fine mesh refinement in the crack tip region would not be strictly required. Nevertheless, we follow similar arrangement already used in our previous analyses [28,60–62] and adopt a conventional mesh configuration having a focused ring of elements surrounding the crack front with a small key-hole of a radius, $\rho_0 = 0.0025$ mm at the crack tip. Symmetry conditions permit modeling of only one-half of the fracture specimens with appropriate constraints imposed on the remaining crack ligament and plane-strain constraints imposed ($w = 0$) on each node. A typical half-symmetric model has one thickness layer with $B = 1$ mm (unit thickness) and contains ~3000 8-node, 3-D elements (~6400 nodes). The finite element models for the SE(B) specimens are loaded by displacement increments imposed on the top nodes for the plane defining the applied load as shown in Fig. 4(a). An analogous scheme is also employed in case of the C(T) specimens with displacement increments applied on the outermost nodes of the pin hole (which also defined a vertical plane containing the applied load) as indicated in Fig. 2(a) – to conserve space, the finite element mesh for this specimen is not shown. Similarly, the finite element models for the clamped SE(T) configurations are loaded by displacement increments imposed on the loading points shown in Fig. 4(b). Because the numerical models of the fracture specimens, including specifically the C(T) geometry and the SE(B) specimens under 3-point and 4-point loading, employ linear elastic elements, there is no need to model the rollers of the bend test fixture or the loading pin, in which case a contact analysis would be required. Our previous numerical experience reveals that such a refinement provides little improvement, if any, in the load-displacement response even in the case of an elastic-plastic analysis.

3.2. 3-D finite element models

Finite element analyses are also conducted on numerical models in full 3-D setting for selected plane-sided fracture specimens, including the C(T) and clamped SE(T) geometries as well as the 3-point SE(B) configuration with $S/W = 4$ described previously. The analysis matrix includes the same crack configurations as defined before covering $a/W = 0.1$ to 0.8 with increments of 0.1. To asses the effects of thickness on specimen elastic compliance, the 3-D numerical computations are performed on finite element models for the C(T) and 3-point SE(B) specimens having $B = 25$ mm (1T configuration). For the SE(T) specimen, the analysis matrix considers a fracture specimen with $B = 15$ mm and $B = W$ configuration with $H/W = 10$ – this geometry represents typical specimen configurations extracted from common pipeline girth welds to measure crack growth resistance curves (see Mathias et al. [30] for an illustrative example). Further, to examine the effects of side-grooves on specimen compliance, we also analyze those fracture specimens already described but for which the numerical models have 20% side-grooves (10% each side). Here, the side-grooves are introduced in the numerical models as follows: (1) the Y-constraints on crack-plane nodes for which $X = 0$ and $Z > 0.4B$ (these nodes correspond to the 4 outermost layers) are first released; (2) these nodes are translated in the Y direction according to a linear mapping corresponding to a side-groove half-angle of 30°. Since the primary interest here lies in the effect of side-grooves on the load-displacement response to determine the specimen compliance, the notch radius of the side-groove is not modeled.

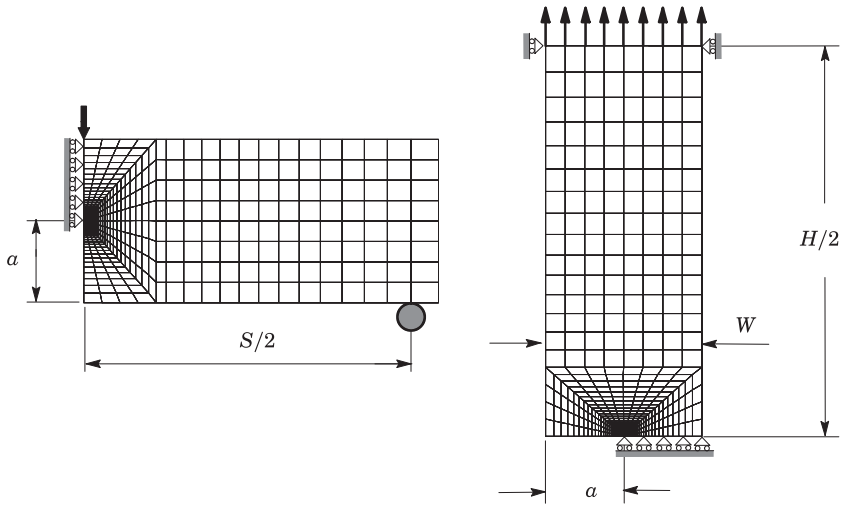

Fig. 4. Typical plane strain, finite element models utilized in the analyses: (a) 3-point SE(B) specimen with $a/W = 0.5$. (b) Clamped SE(T) configuration having $H/W = 10$ with $a/W = 0.5$.

Fig. 5 shows the typical finite element models utilized in the 3-D analyses of the 20% side-grooved 1T C(T) specimen with $a/W = 0.5$ and the plane-sided SE(T) geometry with $W = B = 15$ mm and $a/W = 0.5$. Symmetry conditions enable analyses using one-quarter of the 3-D models with appropriate constraints imposed on the symmetry planes. The meshes have typically 21–27 variable thickness layers defined over the half-thickness $(B/2)$; the thickest layer is defined at $Z = 0$ with thinner layers defined near the free surface $(Z = B/2)$ and the side-groove region $(Z = B_N/2)$ to accommodate strong Z variations in the stress distribution. The quarter-symmetric, 3-D model for these specimens have approximately 25,000–34,000 8-node, 3-D elements. All finite element models are loaded by displacement increments imposed on appropriate nodes as already described in previous section.

3.3. Solution procedures and material properties

The numerical solutions for evaluation of specimen compliance in terms of the evolution of applied load with increased CMOD described here utilize a conventional linear elastic constitutive model to describe the linear elastic tensile response for the material. The mechanical properties adopted in all numerical computations performed on the crack configurations analyzed include Young's modulus, $E = 206$ GPa and Poisson's ratio, $\nu = 0.3$. The finite element code WARP3D [63] provides the numerical solutions for the extensive finite element analyses reported here.

4. Results and discussion

The following sections provide an extensive set of compliance solutions derived from the plane-strain and 3-D numerical analyses conducted on the tensile-loaded and bend specimens previously described. The presentation begins with representative descriptions of the elastic global response in terms of load versus displacement trajectories for selected fracture specimens. New polynomial compliance functions with varying a/W-ratios obtained from plane-strain finite element analyses are then provided and compared with previously reported results. To facilitate manipulation of the compliance quantities

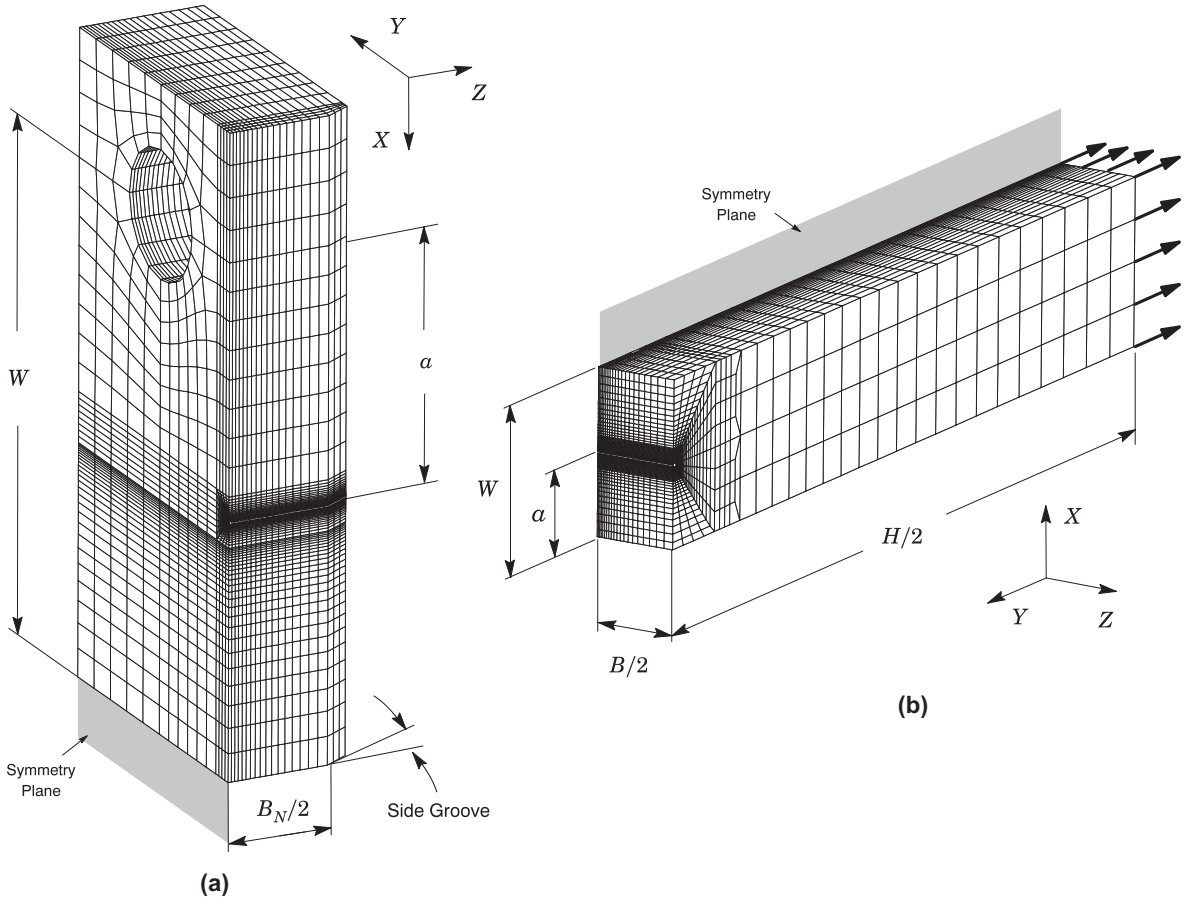

Fig. 5. 3-D finite element models with 20% side-grooves: (a) 1T C(T) specimen having 20% side-groove (10% each side) with $a/W = 0.5$. (b) Plane-sided clamped SE(T) configuration having $a/W = 0.5$ with $W = B = 15$ mm and $H/W = 10$.

relative to the fracture specimens, the numerical solutions are also characterized by tables of numerical values describing the corresponding polynomial coefficients. Finally, attention is directed to 3-D effects on the specimen compliance, including the influence of side-grooves.

4.1. Elastic global response

Before launching into the numerical evaluation of the compliance functions addressed next, we first examine the influence of specimen geometry on the elastic global response in terms of load versus displacement trajectories which has a direct bearing on the evolution of μ with varying a/W-ratios for the crack configurations considered in the present investigation. Since μ derives directly from the variation of specimen compliance, comparison of the relationship between load and CMOD for a given crack size and specimen geometry is also of interest.

Fig. 6 shows the typical variation of applied load with increased CMOD for varying a/W-ratios for selected configurations. The results shown in this figure consider the following key specimen geometries: (a) standard C(T) specimen with a straight notch, (b) clamped SE(T) geometry with $H/W = 10$, (c) standard 3-point SE(B) specimen with $S/W = 4$ and (d) 4-point SE(B) configuration with $S/W = 4$. The relationship between load and crack mouth opening displacement derived from the elastic solution provided by Tada et al. [18] is also included for the C(T) and 3-point SE(B) specimens – these elastic solutions for the C(T) geometry are valid only for $a/W \geqslant 0.2$. Here, we note that the comparisons included in Fig. 6(d) for the 4-point bend geometry are obtained from the $P-$CMOD relationship given in [18] for a single edge notch configuration under pure bending. Moreover, we should also point out that Tada et al. [18] do not provide elastic solutions for the single edge notch tension specimen with fixed grips (clamped ends).

The influence of specimen geometry and loading mode on the elastic global response of the analyzed crack configurations is evident in these plots. As could be expected, the elastic $P-$CMOD curves for all fracture geometries depends strongly on the crack size, particularly for low to moderate a/W-ratios. Observe, however, that the load vs. displacement trajectories for the C(T) specimen are overall lower than the corresponding trajectories for other configurations displayed in Fig. 6. Further observe that the P-CMOD curves for this specimen geometry are somewhat less sensitive to crack size than the other configurations. Moreover, it is of interest to note the apparent effect of the loading mode on the elastic global response for the SE(B) specimens displayed in Fig. 6(c) and (d); here, for a given a/W-ratio and fixed CMOD-value, the applied load is higher for the 4-point SE(B) geometry.

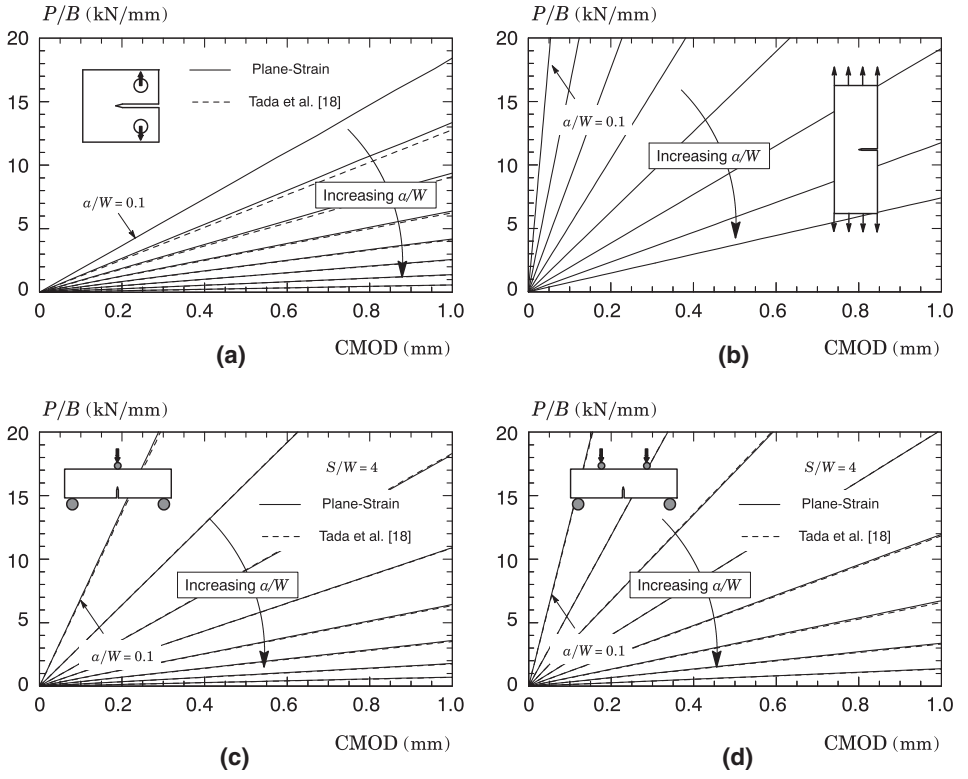

Fig. 6. Variation of applied load with increased CMOD for varying a/W-ratios for selected configurations: (a) C(T) specimen. (b) Clamped SE(T) geometry. (c) 3-point SE(B) specimen with $S/W = 4$. (d) 4-point SE(B) geometry with $S/W = 4$.

The dashed lines shown in Fig. 6(a), (c) and (d) pertain to the elastic solutions provided by Tada et al. [18]. These set of results exhibit very good agreement with our plane-strain analyses, particularly for the bend specimens – here, the $P-$CMOD relationships from [18] essentially collapse onto the plane-strain results for every a/W-ratio considered. The agreement between our analyses and the elastic solutions from Tada et al. [18] for the C(T) specimen is also very good for deeply-cracked geometries in which $a/W \geqslant 0.4$. Further observe that the $P-$CMOD curves obtained from [18] agree rather well with the computed results but they are nevertheless somewhat lower than our plane-strain results.

Comparisons of the P vs. CMOD trajectories for the 3-point bend specimen with different geometry displayed in Fig. 7 further illustrate the effect of S/W-ratio on the elastic load-displacement behavior for this configuration. Not surprisingly, the evolution of load with crack mouth opening displacement for a fixed a/W-ratio is lower with increased S/W-ratio. Essentially similar behavior is also observed for the 4-point bend specimen – to conserve space, these results are not shown here. Furthermore, the relationship between load and CMOD derived from the elastic solution provided by Tada et al. [18] is also included in the plots to aid in assessing the computed results. While we note that the compliance relationships given in Tada et al. [18] are essentially valid for bend specimens with $S/W = 4$, these set of results exhibit general good agreement with our plane-strain analyses.

4.2. Compliance relationships for tensile-loaded specimens

We begin by presenting results for the compliance solutions derived from the numerical analyses conducted on the C(T) and SE(T) specimens described previously. Figs. 8 and 9 shows the variation of normalized compliance, μ, with a/W for these configurations in which μ is defined by Eq. (3). The solid lines represent a polynomial fitting to the numerical results as provided later in Section 4.4. To facilitate comparisons with previously published results, the plots also include compliance solutions from a number of key sources, including applicable fracture toughness and fatigue crack growth test standards.

Fig. 8 shows the dependence of normalized compliance, μ, on a/W for the C(T) configuration. Our results compare well with the compliance formulas given by ASTM E647 [9] and ISO 12135 [53], particular in the range $a/W \geqslant 0.4$. However, we note that there appears to be an error in expression (D.4) of ISO 12135 as the term $\left[1-(a/W)^2\right]$ appearing in the function g_4 should be $[1-(a/W)]^2$ instead. Observe also that the compliance expression of ASTM E647 is essentially valid for $0.2 \leqslant a/W \leq 0.975$.

Fig. 9 displays the variation of normalized compliance, μ, with crack size for the clamped SE(T) specimens. The relationship between μ and a/W derived from the present analysis compares well with recently published results from Cravero and Ruggieri (C&R) [28] and Shen and Tyson (S&T) [29]. For comparison, the figure also includes the evolution of μ with a/W based on prior work of Blatt et al. [20] who conducted 2-D plane-stress finite element analysis to determine compliance solutions for a clamped SE(T) configuration with $H/W = 4$.

4.3. Compliance relationships for bend specimens

Figs. 10 and 11 provide descriptions of specimen compliance with increased a/W-ratios based on the finite element analyses performed on the 3-point and 4-point bend specimens. In each case, the normalized compliance, μ, is defined by Eq. (5) whereas the solid lines denote a polynomial fitting to the numerical results as described subsequently in Section 4.4. Compliance relationships from other published works are also provided in the figures to aid in comparing the current results with previous research.

Consider first the dependence of μ on a/W for the 3-point SE(B) specimen with varying S/W-ratios displayed in Fig. 10. Apart from very minor differences in the μ-levels for a given a/W-ratio (most likely caused by the numerical procedure to extract the specimen compliance), the variation of μ with a/W for every analyzed S/W-ratio is essentially unchanged.

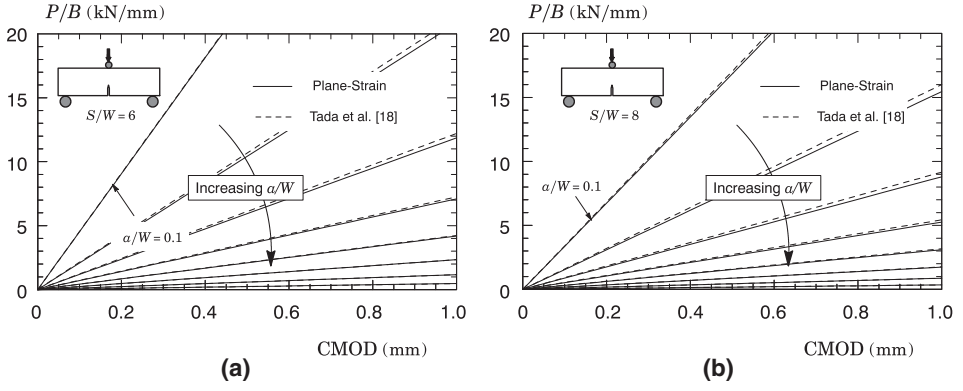

Fig. 7. P vs. CMOD trajectories for the 3-point bend specimen with different geometry: (a) $S/W = 6$. (b) $S/W = 8$.

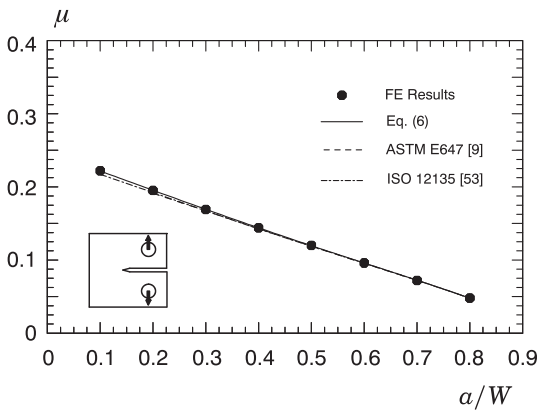

Fig. 8. Dependence of normalized compliance, μ, on a/W for the C(T) configuration.

Further observe that the compliance relationships given by Tada et al. [18] and ASTM E1820 [8] compare well with our numerical results. In this regard to the compliance relationship given by ASTM E1820 [8], it deserves mention that this standard actually provides two compliance solutions for the 3-point bend specimen, albeit similar, in which one corresponds to a deeply cracked geometry $(a/W \geqslant 0.45)$ and the other to shallow cracked specimens $(a/W < 0.45)$ – the dashed line shown in the plot represents those compliance solutions.

Consider next the variation of μ with a/W for the 4-point SE(B) specimen and varying S/W-ratios shown in Fig. 11. The overall trends remain similar except that the levels of specimen compliance, μ, for this configuration are higher compared to the 3-point bend specimen (note that the scale on the y-axis in both plots is slightly different). Also observe that the compliance relationships given by Tada et al. [18] (recall that the $P-$CMOD relationship given in [18] derives from a single edge notch configuration under pure bending) and prior work of Tarafder et al. [24] (which provides compliance relationships for the 4-point bend specimen in the range $0.25 \leqslant a/W \leq 0.8$) compare well with our numerical results.

4.4. Polynomial fitting

The variation of normalized specimen compliance and crack size given by the above numerical results for the specimen geometries analyzed is more easily manipulated by introducing a functional form to describe the compliance relationships. Following widely adopted procedures, a polynomial function to describe the dependence of μ on a/W yields

$$\mu = \alpha_0 + \alpha_1(a/W) + \alpha_2(a/W)^2 + \alpha_3(a/W)^3 + \alpha_4(a/W)^4 + \alpha_5(a/W)^5 \tag{6}$$

where it is understood that a 5th-degree polynomial fitting is employed to obtain the coefficients, α_k.

As already mentioned, a key step in the experimental evaluation of crack growth resistance curves [2,8,28,37] or fatigue crack growth rates [2,9] involves the accurate estimation of the current crack length (as testing progresses) based on experimental measurements of the change in the specimen elastic compliance. Consequently, it is more convenient to manipulate

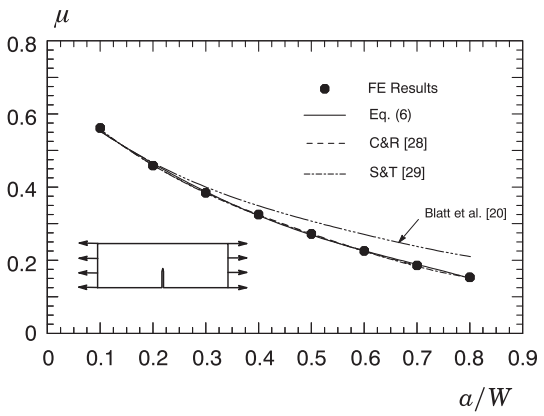

Fig. 9. Variation of normalized compliance, μ, with crack size for the clamped SE(T) specimen with $H/W = 10$.

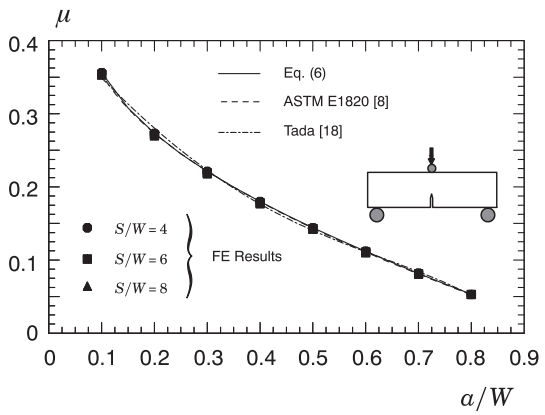

Fig. 10. Dependence of μ on a/W for the 3-point SE(B) specimen with varying S/W-ratios.

the above expression to define the functional dependence of crack length and specimen compliance as the inverse of previous Eq. (6) in the form

$$a/W = \beta_0 + \beta_1\mu + \beta_2\mu^2 + \beta_3\mu^3 + \beta_4\mu^4 + \beta_5\mu^5 \tag{7}$$

Tables 1,2 provide the polynomial coefficients of Eqs. (6) and (7) derived from a standard least square fitting of our numerical results valid in the range $0.1 \leqslant a/W \leq 0.8$. As mentioned earlier, the solid lines displayed in the plots of Figs. 8–11 define the fitting curves corresponding to Eq. (6).

4.5. 3-D effects on specimen compliance

To verify the effects of out-of-plane displacements associated with specimen thickness and side-grooves on the specimen elastic compliance and how it compares with the 2-D μ-values, the present study also considers analyses of 3-D models for the selected fracture specimens. The 3-D finite element models for these specimen geometries were described previously in Section 3.2 and include a 1T C(T) geometry, a standard 1T SE(B) specimen under 3-point bending loading and a clamped SE(T) configuration with $W = B = 15$ mm. The analyses consider plane-sided and 20% (10% each side) side-grooved geometries.

Fig. 12(a)–(c) shows the variation of μ with a/W-ratio derived from the 3-D finite element analyses. Each plot in this figure shows the effects of specimen thickness and side-grooves on specimen compliance and also compares the corresponding dependence of μ on a/W obtained previously from the 2-D computations. The trends are clear. For every case analyzed, the 3-D results, including the normalized compliance values for the side-grooved models, are virtually indistinguishable from the compliance relationship described by Eq. (6) obtained by a 5th-order polynomial fitting to the numerical 2-D results. Similar trends were found for other specimen geometries but these results are not shown here in interest of space. The insensitivity of specimen compliance to thickness and side-grooves exhibited by the plots displayed in Fig. 12(a)–(c) provides an interesting result in that the 2-D compliance relationships are accurately descriptive of the dependence of μ on a/W (and, consequently, the corresponding inverse relationship defining a/W as a function of μ) for the fracture specimens analyzed.

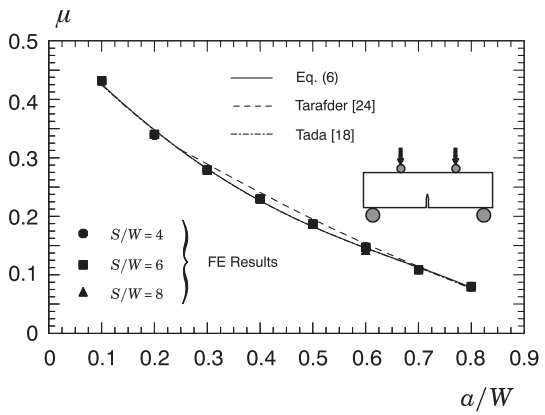

Fig. 11. Variation of μ with a/W for the 4-point SE(B) specimen and varying S/W-ratios.

Table 1
Coefficients for the polynomial fitting of Eq. (6) defining the relationship between μ and a/W.

Specimen	Geometry	α_0	α_1	α_2	α_3	α_4	α_5
C(T)	Straight Notch	0.2487	−0.2593	−0.1304	0.5478	−0.7212	0.3205
Clamped SE(T)	$H/W = 10$	0.7234	−2.0575	5.2243	−9.4590	8.8792	−3.2403
3-Point SE(B)	All S/W	0.5036	−1.9663	5.8823	−11.0250	10.4590	−3.9101
4-Point SE(B)	All S/W	0.5844	−1.9692	5.2353	−8.9261	7.4811	−2.3611

Table 2
Coefficients for the polynomial fitting of Eq. (7) defining the relationship between a/W and μ.

Specimen	Geometry	β_0	β_1	β_2	β_3	β_4	β_5
C(T)	Straight Notch	1.0216	−5.3474	23.9166	−223.4974	954.6388	−1458.8273
Clamped SE(T)	$H/W = 10$	1.7548	−10.7686	43.1621	−108.2553	139.5816	−70.3533
3-Point SE(B)	All S/W	1.0033	−4.0437	4.7902	−13.7062	59.6424	−71.7480
4-Point SE(B)	All S/W	1.3177	−10.2567	65.6950	−271.2962	549.9747	−420.7141

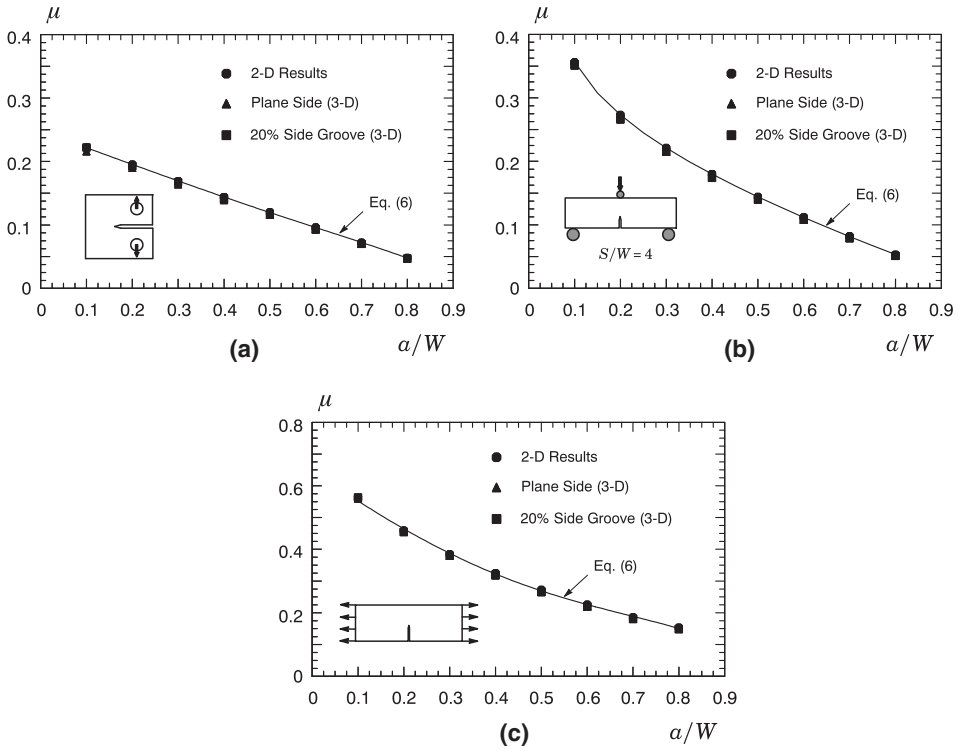

Fig. 12. Variation of μ with a/W-ratio derived from the 3-D finite element analyses, including numerical results for plane-sided and 20% side-grooved models: (a) C(T) specimen. (b) Standard SE(B) geometry with $S/W = 4$. (c) Clamped SE(T) specimen with $H/W = 10$.

4.6. Reconciling 2-D compliance in fracture testing: plane strain vs. plane stress

Thus far, the compliance relationships obtained for the specimen geometries considered here, including the polynomial fitting defined by Eqs. (6) and (7), are derived on the basis of plane-strain analyses performed on 2-D numerical models. As discussed earlier in connection with the presentation given in Section 2, the normalized specimen compliance can be also defined in terms of plane-stress conditions. While the choice of a proper plane state condition may appear somewhat arbitrary, it is interesting to note that it does have some implications in fracture testing, specifically in experimental crack length measurements. This can be understood by the following argument. For a given specimen geometry under plane-stress conditions, the load-displacement relationship with varying crack size, as characterized by the a/W-ratio, is reduced by a factor $1 - \nu^2$ compared to the corresponding load-displacement trajectories under plane-strain conditions (see Figs. 1(b), 6, and 7). Because the specimen is now less stiff, the increased compliance under plane-stress conditions would produce a small

increase in the experimental estimate of crack length (compared to that under plane-strain conditions) obtained during the fracture test thereby resulting in a slightly more conservative fracture resistance curve.

To illustrate this issue, consider additional analyses of the clamped SE(T) and the 3P SE(B) geometries already described in Section 3.1. Fig. 13(a) and (b) displays the evolution of specimen compliance based on CMOD, C_V, with a/W for these two specimen configurations derived from plane-strain and plane-stress analyses. The trends follow exactly those brought out above as the plane-stress $C_V - a/W$ curves lie above the corresponding curves for plane-strain conditions. However, while one could be attempted to favor plane-stress analysis to describe the compliance relationships for use in fracture testing, the choice of a given plane state condition to estimate crack length has no practical consequences since it is always possible to generate crack length estimates either in plane-stress or plane-strain conditions by simply manipulating the way the specimen compliance is normalized.

For the present analysis, the simplest way of considering plane-stress conditions in crack length measurements and, at the same time, using the compliance relationships developed in the present work (which pertain to plane strain conditions) is to note that the normalized specimen compliance, μ, given by Eqs. (3) and (5) can also be defined by $E' = E$ rather than $E' = E/(1 - \nu^2)$. Hence, the experimentally measured specimen compliance, C, can be used in connection with the substitution of the plane-stress modulus, E, into the expression defining the functional dependence of crack length and μ given by previous Eq. (7) to arrive at the plane-stress estimate of crack length. A similar approach is also adopted in ASTM E1820 [8] to determine the experimental crack length for the single specimen test method using the elastic compliance technique. More recent versions of this standard define the functional dependence of crack length and specimen compliance by a 5th-degree polynomial fitting with the same polynomial coefficients already given by older versions (see, *e.g.*, Ref. [64]), but with $E/(1 - \nu^2)$ replaced by E to define the normalized specimen compliance, μ.

5. Summary and conclusions

The extensive linear finite element analyses in 2-D and 3-D of various fracture specimens performed in this investigation provide a larger, new set of normalized specimen compliance solutions which serve to evaluate crack length changes in conventional fracture toughness and fatigue crack growth tests. The study covered selected standard and non-standard fracture test specimens, including the compact tension C(T) configuration, the single edge notch tension SE(T) specimen with fixed-grip loading (clamped ends) and the single edge notch bend SE(B) geometry with varying specimen span over width ratio and loaded under 3-point and 4-point flexural configuration. The results identify improved compliance solutions spanning a wide range of crack sizes as characterized by the a/W-ratio.

In applications to date, these compliance solutions are simply used to correlate the changes in specimen compliance (or stiffness) with the amount of increased stable crack growth during the fracture test. Presumably, since these compliance relationships are entirely derived from elastic analyses, the experimental crack length estimates may be expected to be not fully insensitive to the development of plasticity prior to each unloading-reloading cycle during the fracture resistance test, particularly after the onset of stable crack growth, in which case ductile tearing coupled with the development of background plasticity may affect the actual specimen compliance as suggested in the study of Verstraete et al. [31]. Moreover, it may be noted from the results of this paper that, since the variation of specimen compliance on a/W does depend on the specimen geometry, it may well be possible that the sensitivity of a/W on C could affect the accuracy of crack length measurement depending on the tested specimen geometry. For example, Figs. 10 and 11 show that, for a given range of crack extension such as, for example, from $a/W = 0.3$ to $a/W = 0.4$, the corresponding variations in μ for the 3P and 4P bend specimens are different thereby suggesting a potential effect on crack length measurements. While these issues were not pursued

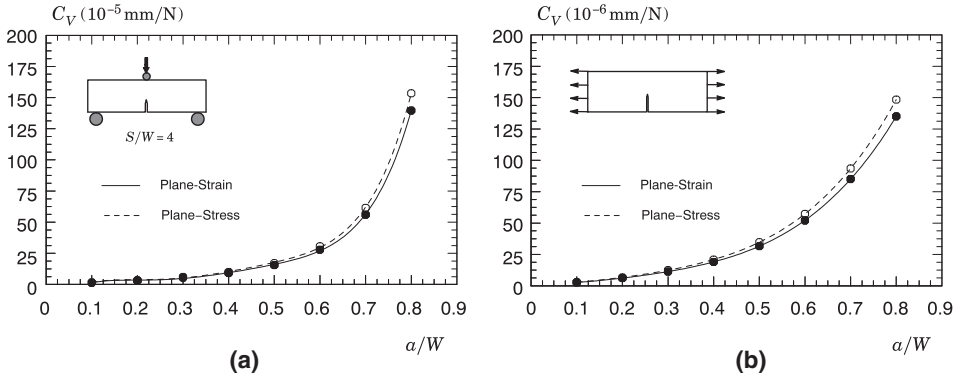

Fig. 13. Evolution of specimen compliance based on CMOD, C_V, with a/W for two specimen geometries derived from plane-strain and plane-stress analyses: (a) Standard SE(B) geometry with $S/W = 4$. (b) Clamped SE(T) specimen with $H/W = 10$.

in this brief study as they need more careful assessment, it is hoped that work along these lines of investigation is encouraged.

The present analysis provides further support to recent standardization efforts to expand and improve current fracture test procedures. In particular, ASTM Task Group E0.8 has commenced on the development of a fracture resistance testing method based on clamped SE(T) specimens which will facilitate fitness-for-service assessment analyses of pipeline girth welds. Moreover, it is also believed that the present set of results can greatly contribute to future revisions of fatigue crack growth test procedures. Overall, the extensive numerical analyses conducted here provide a large set of compliance solutions, which not only validate the compliance relationships available in existing standards such as ASTM E1820 [8], but also help consolidating elastic compliance functions of common specimen geometries for use in routine test procedures for experimental evaluations of crack size changes in fracture toughness and fatigue crack growth testing.

Acknowledgments

This investigation is supported by the Brazilian Council for Scientific and Technological Development (CNPq) through research grant 456222/2013-8. The first author (RFS) would like to acknowledge the financial support from Coordenação de Aperfeiçoamento de Pessoal de Nível Superior (CAPES – Brazil). The work of CR is also supported by the Brazilian Council for Scientific and Technological Development (CNPq) through grant 306193/2013-2.

References

[1] Hutchinson JW. Fundamentals of the phenomenological theory of nonlinear fracture mechanics. J Appl Mech 1983;50:1042–51.
[2] Anderson TL. Fracture mechanics: fundamentals and applications. 3rd ed. Boca Raton, FL: CRC Press; 2005.
[3] Wästberg S, Pisarski H, Nyhus B. Guidelines for engineering critical assessments for pipeline installation methods introducing cyclic plastic strain. In: 23rd international conference on offshore mechanics and arctic engineering (OMAE), Vancouver, Canada; 2004.
[4] Chis T. The mechanics of pipeline reeling. Fascicle of management and technological engineering, vol. VI (XVI). Oradea University; 2007. p. 617–25.
[5] Manouchehri S, Howard B, Denniel S. A discussion of the effect of the reeled installation process on pipeline limit states. In: 18th international offshore and polar engineering conference (ISOPE), Vancouver, Canada; 2008.
[6] Manouchehri S. A discussion of practical aspects of reeled flowline installation. In: 31st international conference on ocean, offshore and arctic engineering (OMAE 2012). Rio de Janeiro (Brazil): American Society of Mechanical Engineers; 2012.
[7] Cosham A, Macdonald KA. Fracture control in pipelines under high plastic strain – a critique of DNV-RP-F108. In: 7th international pipeline conference (IPC 2008), Calgary, Canada; 2008.
[8] American Society for Testing and Materials. Standard test method for measurement of fracture toughness. ASTM E1820-15; 2015.
[9] American Society for Testing and Materials. Standard test method for measurement of fatigue crack growth rates. ASTM E647-08; 2008.
[10] Marsh KJ, Smith RA, Ritchie RO, editors. Fatigue crack measurement: techniques and applications. Engineering Materials Advisory Services; 1991.
[11] Xu Y, Gregson PJ, Sinclair I. Systematic assessment and validation of compliance-based crack closure measurements in fatigue. Mater Sci Eng A 2000;284:114–25.
[12] Skorupa M, Machniewicz T, Skorupa A. Applicability of the ASTM compliance offset method to determine crack closure levels for structural steels. Int J Fatigue 2007;29:1434–51.
[13] Sarzosa S, Godefroid LB, Ruggieri C. Fatigue crack growth assessments in welded components including crack closure effects: experiments and 3-D numerical modeling. Int J Fatigue 2013;47:279–91.
[14] Saxena A, Hudak SJ. Review and extension of compliance information for common crack growth specimens. Int J Fract 1978;14(5):453–68.
[15] Wu SX. Crack length calculation formula for three-point bend specimens. Int J Fract 1984;24:R33–5.
[16] Haggag FM, Underwood JH. Compliance of a three-point bend specimen at load line. Int J Fract 1984;26:R63–5.
[17] Underwood JH, Kapp JA, Baratta FI. More on compliance of a three-point bend specimen. Int J Fract 1985;28:R41–5.
[18] Tada H, Paris PC, Irwin GR. The stress analysis of cracks handbook. 3rd ed. American Society of Mechanical Engineers; 2000.
[19] Papaspyropoulos V, Ahmad J. Elastic compliance and stress intensity factor solutions for compact tension geometries. Technical report AFWAL-TR-82-4199. Wright-Patterson AFB, Ohio: Air Force Wright Aeronautical Laboratories; 1983.
[20] Blatt D, John R, Coker D. Stress intensity factor and compliance solutions for a single edge notched specimen with clamped ends. Eng Fract Mech 1994;47(4):521–32.
[21] Tobler RL, Carpenter WC. A numerical and experimental verification of compliance functions for compact specimens. Eng Fract Mech 1985;21(3):547–56.
[22] Jablonski DA, Journet B, Vecchio RS, Hertzberg RW. Compliance functions for various fracture mechanics specimens. Eng Fract Mech 1985;22(5):819–27.
[23] Kapp JA, Leger GS, Gross B. Wide-range displacement expressions for standard fracture mechanics specimens. In: Kanninen MF, Hopper AT, editors. Fracture mechanics: 16th conference. ASTM STP 868. Philadelphia: American Society for Testing and Materials; 1985. p. 27–44.
[24] Tarafder S, Tarafder M, Ranganath VR. Compliance crack length relations for the four-point bend specimen. Eng Fract Mech 1994;47(6):901–7.
[25] John R. Stress intensity factor and compliance solutions for an eccentrically loaded single edge cracked geometry. Eng Fract Mech 1997;58(1–2):87–96.
[26] Guinea GV, Pastor JY, Planas J, Elices M. Stress intensity factor, compliance and CMOD for a general three-point-bend beam. Int J Fract 1998;89:103–16.
[27] Joyce JA, Hackett EM, Roe C. Effects of crack depth and mode loading on the J-R curve behavior of a high strength steel. In: Underwood JH, Schwalbe K-H, Dodds RH, editors. Constraint effects in fracture. ASTM STP 1171. Philadelphia: American Society for Testing and Materials; 1993. p. 239–63.
[28] Cravero S, Ruggieri C. Estimation procedure of J-resistance curves for SE(T) fracture specimens using unloading compliance. Eng Fract Mech 2007;74:2735–57.
[29] Shen G, Tyson WR. Crack size evaluation using unloading compliance in single-specimen single-edge notched tension fracture toughness testing. J Test Eval 2009;37(4):347–57.
[30] Mathias LLS, Sarzosa DFB, Ruggieri C. Effects of specimen geometry and loading mode on crack growth resistance curves of a high-strength pipeline girth weld. Int J Press Vessels Pip 2013;111–112:106–19.
[31] Verstraete MA, Hertelé S, Denys RM, Van Minnebruggen K, De Waele W. Evaluation and interpretation of ductile crack extension in sent specimens using unloading compliance technique. Eng Fract Mech 2014;115:190–203.
[32] Sarzosa DFB, Barbosa VS, Santos CP, Hippert E, Ruggieri C. Fracture resistance testing of dissimilar nickel-chromium girth welds for clad line pipes. Int J Fract 2017;205(2):168–88.
[33] Kanninen MF, Popelar CH. Advanced fracture mechanics. New York: Oxford University Press; 1985.
[34] Hutchinson IW, Paris PC. Stability analysis of *J*-controlled crack growth. In: Landes JD, Begley JA, Clarke GA, editors. Elastic-plastic fracture. ASTM STP 668. Philadelphia: American Society for Testing and Materials; 1979. p. 37–64.

[35] Ernst HA, Paris PC, Landes JD. Estimations on *J*-integral and tearing modulus *T* from a single specimen test record. In: Roberts R, editor. Fracture mechanics: thirteenth conference. ASTM STP 743. Philadelphia: American Society for Testing and Materials; 1981. p. 476–502.
[36] Cravero S, Ruggieri C. Further developments in *J* evaluation procedure for growing cracks based on LLD and CMOD data. Int J Fract 2007;148:387–400.
[37] Joyce JA. Manual on elastic-plastic fracture: laboratory test procedure. ASTM manual series MNL 27. ASTM International; 1996.
[38] Zhu XK, Joyce JA. Review of fracture toughness (*G*, *K*, *J*, CTOD, CTOA) testing and standardization. Eng Fract Mech 2012;86:1–46.
[39] Faucher B, Tyson WR. A comparison of crack-mouth opening and load-line displacement for *J*-integral evaluation using bend specimens. In: Wessel ET, Loss FJ, editors. Elastic-plastic fracture test methods. ASTM STP 856. Philadelphia: American Society for Testing and Materials; 1985. p. 278–93.
[40] Saxena A. Nonlinear fracture mechanics for engineers. Boca Raton: CRC Press; 1998.
[41] American Society for Testing and Materials. Standard terminology relating to fatigue and fracture testing. ASTM E1823-2013; 2013.
[42] Ernst HA, Paris PC, Landes JD. Estimations on *J*-integral and tearing modulus *T* from a single specimen record. In: Roberts R, editor. Fracture mechanics: thirteenth conference. ASTM STP 743. Philadelphia: American Society for Testing and Materials; 1981. p. 476–502.
[43] Sumpter JDG, Turner CE. Method for laboratory determination of jc. In: Swedlow JL, Williams ML, editors. Cracks and fracture. ASTM STP 601. Philadelphia: American Society for Testing and Materials; 1976. p. 3–18.
[44] Zhu XK, Leis BN, Joyce JA. Experimental estimation of *J-R* curves from load-CMOD record for SE(B) specimens. J ASTM Int 2008;5(5):1–15.
[45] Kirk MT, Dodds RH. *J* and CTOD estimation equations for shallow cracks in single edge notch bend specimens. J Test Eval 1993;21:228–38.
[46] Nyhus B, Polanco M, Ørjasæter O. SENT specimens as an alternative to SENB specimens for fracture mechanics testing of pipelines. In: 22nd international conference on ocean, offshore and arctic engineering (OMAE), Vancouver, Canada; 2003.
[47] Cravero S, Ruggieri C. Correlation of fracture behavior in high pressure pipelines with axial flaws using constraint designed test specimens – Part I: plane-strain analyses. Eng Fract Mech 2005;72:1344–60.
[48] Silva LAL, Cravero S, Ruggieri C. Correlation of fracture behavior in high pressure pipelines with axial flaws using constraint designed test specimens – Part II: 3-D effects on constraint. Eng Fract Mech 2006;76:2123–38.
[49] Shen G, Bouchard R, Gianetto JA, Tyson WR. Fracture toughness evaluation of high-strength steel pipe. In: ASME PVP 2008 pressure vessel and piping division conference. Chicago, IL: American Society of Mechanical Engineers; 2008.
[50] Veritas Det Norske. Fracture control for pipeline installation methods introducing cyclic plastic strain. DNV-RP-F108; 2006.
[51] British Institution. Method of test for determination of fracture toughness in metallic materials using single edge notched tension (SENT) specimens. BS 8571; 2014.
[52] British Standard. Fracture mechanics toughness tests – Part 1. Method for determination of K_{Ic}, critical CTOD and critical *J* values of metallic materials. BS 7448-1:1991; 1991.
[53] International Organization for Standardization. Metallic materials – unified method of test for the determination of quasistatic fracture toughness. ISO 12135-2002; 2002.
[54] Grabowski I, Yates JR. The effect of specimen geometry on short-crack growth behavior of a nickel-based superalloy. Int J Fatigue 1992;14(4):227–32.
[55] Yates JR, Zhang W, Miller KJ. The initiation and propagation behavior of short fatigue cracks in Waspaloy subjected to bending. Fatigue Fract Eng Mater Struct 1993;16(3):351–62.
[56] Campbell JP, Ritchie RO. Mixed-mode, high-cycle fatigue-crack growth thresholds in Ti-6Al-4V – I: a comparison of large and short crack behavior. Eng Fract Mech 2000;67:209–27.
[57] Kobayashi H, Konda N, Sutep JAK, Horikawa K, Yamauchi T. Fatigue crack extension in four-point bending test for steels imitated heat affected zone. J Soc Mater Sci Jpn 2015;64(4):323–9.
[58] Craig RR. Mechanics of materials. New York, NY: John Wiley & Sons; 1996.
[59] Gere JM. Mechanics of materials. 6th ed. Toronto, Canada: Cengage Learning; 2006.
[60] Ruggieri C. Further results in *J* and CTOD estimation procedures for SE(T) fracture specimens – Part I: homogeneous materials. Eng Fract Mech 2012;79:245–65.
[61] Savioli RG, Ruggieri C. *J* and CTOD estimation formulas for C(T) fracture specimens including effects of weld strength overmatch. Int J Fract 2013;179:109–27.
[62] Souza RF, Ruggieri C. Revised η-factors and *J*-CTOD relationships for SE(B) fracture specimens including 3-D effects and implications for fracture toughness measurements. Mater Perform Characteriz 2015;2(2):34–54. ASTM International.
[63] Healy B, Gullerud A, Koppenhoefer K, Roy A, RoyChowdhury S, Petti J, et al. WARP3D: 3-D nonlinear finite element analysis of solids for fracture and fatigue processes. Tech. rep. University of Illinois at Urbana-Champaign; 2014. <http://code.google.com/p/warp3d>.
[64] American Society for Testing and Materials. Standard test method for measurement of fracture toughness. ASTM E1820-96; 1996.